

**SIMULATION, FABRICATION AND CHARACTERIZATION OF
MULTILAYER COATED SOLAR CELLS**

by

WISAM J. AZIZ

**Thesis submitted in fulfillment of the requirements for the degree of
Doctor of Philosophy**

January 2011

ACKNOWLEDGEMENTS

In the name of Allah, Most Gracious, Most Merciful

First of all, I would like to thank Allah for granting me health, patience, and determination to complete this doctoral study. I would also like to thank my supervisor Professor Dr. Kamarulazizi Ibrahim for his guidance, time, moral support, and critical questions about my research. I consider myself very lucky and most honored to have been one of his students.

A special thank goes to the professional editor, Mr. Ghayth al-Shaibani for his valuable academic comments and editing.

The prayers of my father and mother, the patience of my wife, Rana and my three daughters, Hajar, Sara, and Retage and the support of my brothers and sisters, were a powerful source for my success.

I also appreciate the help and support offered by the Dean of School of Physics Professor Dr. Zainuriah Hassan.

I would also like to thank all the technical assistants in NOR-LAB/USM for their help in the laboratory while conducting my research.

Eventually, I thank all my friends and colleagues who supported me and helped me at the School of Physics / Universiti Sains Malaysia.

TABLE OF CONTENTS

Page	
ACKNOWLEDGEMENTS	ii
TABLE OF CONTENTS	iii
LIST OF TABLES	viii
LIST OF FIGURES	ix
LIST OF ABBREVIATIONS	xv
LIST OF SYMBOLS	xvi
ABSTRAK	xviii
ABSTRACT	xx

CHAPTER 1: INTRODUCTION

1.0	Overview	1
1.1	Materials consideration	2
1.1.1	Bandgap energy	2
1.1.2	Absorption	4
1.1.2.1	Absorption in direct bandgap	4
1.1.2.2	Absorption in an indirect bandgap	6
1.1.3	Multilayer	7
1.2	Rules of device structure	8
1.2.1	Single-junction solar cell	10
1.2.1.1	Homojunction	10
1.2.1.2	Heterojunction	11
1.2.2	Multi-junction solar cell (tandem solar cell)	11
1.3	Simulation as a tool	12
1.4	Research motivations	14
1.5	Objectives of the study	15
1.5.1	Simulation goals	15
1.5.2	Experimental goals	16
1.6	Originality	16
1.7	Outline of the thesis	17

CHAPTER 2: LITERATURE REVIEW

2.0	Introduction	18
2.1	Simulation programs	18
2.2	Multilayer coating techniques	20
2.2.1	Texturing	20
2.2.2	Antireflection coating	21

CHAPTER 3: THEORETICAL FRAMWORK OF SOLAR CELL

3.0	Introduction	24
3.1	Electromagnetic spectrum	24
3.2	The band theory of a solid state	25
3.3	Resistance	26
3.3.1	Shunt resistance	27
3.3.2	Series resistance	28
3.4	Electric field	29
3.5	N-type semiconductors	29
3.6	P-type semiconductors	30
3.7	The p-n junctions in semiconductors	31
3.8	Solar cell principles	34
3.8.1	Overview	34
3.8.2	Short circuit	36
3.8.3	Open circuit	36
3.8.4	Photocurrent	37
3.8.5	Photovoltage	38
3.8.6	Fill factor	38
3.8.7	Efficiency	39
3.9	The optical losses	40
3.9.1	Antireflection coating processes	41
3.9.2	The surface texturing	42
3.9.3	Losses due to non-absorbed light	43
3.9.4	Shadow	44
3.10	Lattice matching	45

CHAPTER 4: NUMERICAL SIMULATION

4.0	Introduction	46
4.1	Basic equations of semiconductor device simulation	49
4.2	Simulation processes	51
4.2.1	The design creating	52
4.2.2	Contacts setting	53
4.2.3	Doping and editing the refinement	53
4.2.4	Creating the final mesh	54
4.2.5	Input files	55
4.2.6	The outputs exhibition	55

CHAPTER 5: INSTRUMENTS

5.0	Introduction	57
5.1	Oxidation and diffusion furnace	57
5.2	Deposition systems	58
5.2.1	Thermal evaporator system	58
5.2.2	Sputtering system	60
5.3	The structural measurement equipment	61
5.3.1	Atomic force microscopy	61
5.3.2	Scanning electron microscopy	62
5.4	The optical measurement equipment	64
5.4.1	Photoluminescence	64
5.4.2	Raman spectroscopy	65
5.4.3	Filmetrics	66
5.5	The electrical measurement equipment	67
5.5.1	Hot probe	68
5.5.2	Hall Effect	69
5.5.3	Current-voltage equipment	69
5.6	The computer's properties	71

CHAPTER 6: EXPERIMENTAL METHODOLOGY

6.0	Introduction	72
6.1	Silicon wafer preparation	73

6.2	Processing of solar cell fabrication	74
	6.2.1 RCA cleaning	76
	6.2.2 Oxidation (silicon dioxide)	77
	6.2.3 Photoresist	77
	6.2.4 Doping	78
	6.2.5 Removing the edge shunt	78
	6.2.6 Texturing	79
	6.2.7 Contact metallization	80
	6.2.8 Annealing process	80
	6.2.9 Antireflection coating (ARC)	81
CHAPTER 7: RESULTS AND DISCUSSION		
7.0	Introduction	84
7.1	Simulating porous silicon as an antireflection coating	84
7.2	Experimental study of multi-structure c-Si solar cells	87
	7.2.1 Texturing	88
	7.2.2 Antireflection coating	107
	7.2.3 Alkaline and acidic texturing with ZnO/TiO ₂ coating	111
	7.2.4 Porous silicon as antireflection coating	115
	7.2.4.1 Porous silicon p-type (100)	116
	7.2.4.2 Porous silicon n-type (100)	119
	7.2.5 Double antireflection structure with back reflector	125
7.3	Concluding remarks	133
8.1	CHAPTER 8: CONCLUSIONS AND FUTURE STUDIES	
8.2	Conclusions	138
	Future studies	139
	REFERENCES	141
	LIST OF PUBLICATIONS	150

LIST OF TABLES

	Page
Table 7.1: Simulation calculations of the fill factor and efficiency of c-Si and PS under input power of 84 mW/cm ² .	87
Table 7.2: Fill factor and efficiency of silicon as grown (c-Si), KOH and acidic texturing with ZnO/TiO ₂ coating.	114
Table 7.3: The fill factor and efficiency of the PS layers based on n-type (100) and p-type (100) wafers with input power 80 mA/cm ² .	125
Table 7.4: Current-voltage measurement of the c-Si and acidic texturing for n-type (100) and antireflection coating ZnO/TiO ₂ at the top and PS as a back reflector.	133
Table 7.5: Summery of the surfaces roughness of samples in this study.	134
Table 7.6: The open circuit voltage, short current density, fill factor and efficiency of samples under this study.	136

LIST OF FIGURES

	Page
Figure 1.1: Bandgap of some common semiconductors materials.	3
Figure 1.2: Energy versus crystal momentum in a direct and indirect bandgap.	5
Figure 1.3: Spectrum-splitting schemes to achieve high conversion efficiencies.	7
Figure 1.4: The generation and recombination phenomenon in semiconductors.	9
Figure 1.5: Multi-junction solar cell design.	12
Figure 3.1: Electromagnetic spectrum of cosmic rays.	24
Figure 3.2: The energy bandgap in insulator, semiconductor and conductor materials.	26
Figure 3.3: The effect of shunt resistance on the current-voltage properties of a solar cell.	28
Figure 3.4: The effect of series resistance on current-voltage properties of a solar cell.	29
Figure 3.5: N-type doping in semiconductor materials.	30
Figure 3.6: P-type doping in semiconductor materials.	31
Figure 3.7: The p-n junction in semiconductor materials.	32
Figure 3.8: Depletion region in p-n junction.	33
Figure 3.9: Photo-generation of the electron-hole pair in p-n junction.	35
Figure 3.10: A typical dark and illuminated solar cell from J–V curve.	39
Figure 3.11: Sources of optical loss in a solar cell.	40
Figure 3.12: The use of a quarter wavelength anti-reflection coating to reduce the surface reflection.	42
Figure 3.13: Radiation paths for a textured silicon surface.	43
Figure 3.14: Light trapping using a randomized reflector on the rear of the cell.	44
Figure 4.1: The typical design of ISE-TCAD simulator.	48

Figure 4.2:	Flow chart of simulation steps of a solar cell.	52
Figure 4.3:	The design creating.	53
Figure 4.4:	The final mesh in ISE-TCAD simulator.	54
Figure 4.5:	Main window of INSPECT showing the work areas.	56
Figure 5.1:	Temperature and time control in the oxidation and diffusion furnace.	58
Figure 5.2:	The thermal evaporator equipment: (a) the whole device, (b) the deposition chamber diagram of the evaporator.	59
Figure 5.3:	D.C sputtering system.	60
Figure 5.4:	Fiber interferometer AFM system.	61
Figure 5.5:	The scheme of a typical SEM system.	63
Figure 5.6:	Filmetrics system model (F20).	67
Figure 5.7:	Hot probe configuration.	68
Figure 5.8:	The current-voltage circuit of solar cell.	70
Figure 5.9:	Current–voltage and power–voltage solar cell characteristics, showing maximum power point (knee of the curve).	70
Figure 6.1:	Flow chart of experimental multilayer coating of the solar cells.	72
Figure 6.2:	The cutter machine of semiconductor wafers.	73
Figure 6.3:	Flow chart of the solar cell fabrication processes.	75
Figure 6.4:	The grid geometry of the front metal mask.	80
Figure 6.5:	The furnace used for contacts annealing.	81
Figure 6.6:	The electrochemical etching cell set-up.	82
Figure 7.1:	Thickness of the c-Si solar cell.	85
Figure 7.2:	Thickness of the PS solar cell.	85
Figure 7.3:	The conduction and valence band energy in the c-Si and PS solar cells.	86

Figure 7.4:	Current density-voltage characteristics of the PS formed on the c-Si.	87
Figure 7.5:	The SEM images of KOH etching of the c-Si p-type (100) for a:5, b:10, c:15, d:20 and e:25 minutes.	89
Figure 7.6:	The reflectance spectra through KOH etching of the c-Si p-type (100) for 5, 10, 15, 20 and 25 minutes.	90
Figure 7.7:	The SEM images of acidic etching of the c-Si p-type (100) for a:5, b:10, c:15, d:20 and e:25 minutes.	91
Figure 7.8:	The reflectance spectra through acidic etching of the c-Si p-type (100) for 5, 10, 15, 20 and 25 minutes.	92
Figure 7.9:	The SEM images of KOH etching of the c-Si p-type (111) for a:5, b:10, c:15, d:20 and e:25 minutes.	93
Figure 7.10:	The reflectance spectra through KOH etching of the c-Si p-type (111) for 5, 10, 15, 20 and 25 minutes.	94
Figure 7.11:	The SEM images of acidic etching of the c-Si p-type (111) for a:5, b:10, c:15, d:20 and e:25 minutes.	95
Figure 7.12:	The reflectance spectra through acidic etching of the c-Si p-type (111) for 5, 10, 15, 20 and 25 minutes.	96
Figure 7.13:	The SEM images of KOH etching of the c-Si n-type (111) for a:5, b:10, c:15 and d:20 minutes.	97
Figure 7.14:	The reflectance spectra through KOH etching of the c-Si n-type (111) for 5, 10, 15, and 20 minutes.	98
Figure 7.15:	The SEM images of acidic texturing of the c-Si n-type (111) for a:5, b:10 and c:15 minutes.	99
Figure 7.16:	The reflectance spectra through acidic texturing of the c-Si n-type (111) for 5, 10 and 15 minutes.	100
Figure 7.17:	The SEM images of KOH of the c-Si n-type (100) for a:5, b:10, c:15 and d:20 minutes.	101
Figure 7.18:	The reflectance spectra of KOH of the c-Si n-type (100) for 5, 10, 15, and 20 minutes.	102
Figure 7.19:	The SEM images of acidic etching of the c-Si n-type (100) for a:5, b:10 and c:15 minutes.	103
Figure 7.20:	The reflectance spectra of acidic etching of the c-Si n-type (100) for 5, 10, and 15 minutes.	104

Figure 7.21:	Reflectivity spectra via acidic texturing for c-Si n-type (100) for 10 minutes and alkaline texturing for c-Si p-type (100) for 25 minutes.	105
Figure 7.22:	AFM images of the silicon surface as grown (c-Si).	106
Figure 7.23:	AFM images of the c-Si n-type (100) surface texturing prepared by acidic etching for 10 minutes.	106
Figure 7.24:	AFM images of the c-Si p-type (100) surface texturing prepared by KOH etching for 25 minutes.	107
Figure 7.25:	The behavior of refractive indices along the distance from the surface of (a) without an ARC (b) with a SiO ₂ coating (c) with a ZnO/TiO ₂ coating.	108
Figure 7.26:	SEM image of the SiO ₂ surface coating.	109
Figure 7.27:	SEM image of the ZnO/TiO ₂ surface coating.	109
Figure 7.28:	AFM images of single layer SiO ₂ .	110
Figure 7.29:	AFM images of double layer ZnO/TiO ₂ .	110
Figure 7.30:	The reflectivity spectra as a function to wavelength of c-Si, SiO ₂ coating and ZnO/TiO ₂ coating.	111
Figure 7.31:	Designs of ZnO/TiO ₂ coating with effective texturing, (a) acidic texturing based on c-Si n-type (100) for 10 minutes (b) alkaline texturing based on c-Si p-type (100) for 25 minutes.	112
Figure 7.32:	The optimal reflectance spectra of alkaline texturing for c-Si p-type (100) for 25 minutes and acidic texturing for c-Si n-type (100) for 10 minutes and ZnO/TiO ₂ antireflection coating.	113
Figure 7.33:	Current density-voltage characteristics of KOH and acidic texturing and ZnO/TiO ₂ coating based on c-Si n-type (100).	114
Figure 7.34:	The reflectance spectra of PS based on different types and orientations of c-Si	115
Figure 7.35:	A cross section image of the PS layer as antireflection coating based on the c-Si p-type (100).	117
Figure 7.36:	A SEM image of the PS based on c-Si p-type (100).	117
Figure 7.37:	AFM images of the PS based on c-Si p-type (100).	118

Figure 7.38:	Photoluminescence spectra of the PS based on c-Si p-type (100) and acidic texturing for c-Si n-type (100) for 10 minutes.	119
Figure 7.39:	A cross section image of the PS layer as top antireflection coating based in the c-Si n-type (100).	120
Figure 7.40:	SEM image of the PS as antireflection coating based on the c-Si n-type (100) wafer.	120
Figure 7.41:	AFM images of PS based on the c-Si n-type (100) wafer.	121
Figure 7.42:	A comparison between the reflectivity of the present work for the PS p-type (100) and PS n-type (100).	122
Figure 7.43:	Raman spectra of the PS p-type (100) and PS n-type (100), and c-Si samples.	123
Figure 7.44:	PL spectra of n-type and p-type of the PS prepared by electrochemical etching.	123
Figure 7.45:	Current density-voltage curve of the PS layers based on c-Si n-type (100) and p-type (100).	125
Figure 7.46:	The design of the PS as a back reflector coating and the acidic texturing for c-Si n-type (100) for 10 minutes and (ZnO/TiO ₂) coating on the top side of the solar cell.	126
Figure 7.47:	SEM image of the PS formed on the unpolished back side of c-Si n-type (100) wafer.	127
Figure 7.48:	SEM images (cross-section) of the PS formed on the unpolished back side of c-Si n-type (100) wafer.	128
Figure 7.49:	Schematic incident light on a c-Si solar cell with AR, texturing and reflection coating.	129
Figure 7.50:	AFM images of the PS as reflector at the back side.	130
Figure 7.51:	The reflectance spectrum of the back side of the PS prepared by electrochemical etching.	130
Figure 7.52:	PL spectrum of the back side of the PS prepared by electrochemical etching.	131
Figure 7.53:	Current density voltage curve of ZnO/TiO ₂ and acidic texturing at the top and PS as a reflection coating at the rear.	132
Figure 7.54:	Solar cell structure of Zhang, et al. (2006) consists of ZnO/Ag/Al as a back reflector coating.	132

LIST OF ABBREVIATIONS

AFM	Atomic force microscope
AM1.5	Air mass of global irradiance spectrums
ARC	Antireflection coating
CVD	Chemical vapour deposition
CO	Carbon oxide
CO ₂	Carbon dioxide
CH ₃ COOH	Acetic acid
HF	Hydrofluoric acid
HNO ₃	Hydrogen nitrate or nitric acid
FF	Fill factor
KOH	Potassium hydroxide
MBE	Molecular beam epitaxy
MOCVD	Metalorganic chemical vapor deposition
NH ₄ F	Ammonium fluoride
PL	Photoluminescence spectra
PS	Porous silicon
QW	Quantum well
R _{SH}	Shunt resistance
R _S	Series resistance
rpm	Revolutions per minute (r/min)
SEM	Scanning electron microscopy
Si	Silicon
SiO ₂	Silicon dioxide
SiOH	Silicon hydroxide
TiO ₂	Titanium dioxide
UV	Ultra violet
ZnO	Zinc oxide

LIST OF SYMBOLS

D_0	Solar constant
D_n, D_p	Diffusion constant of electron and hole
E_g	Energy bandgap
E_D, E_A	The values of the doping levels
E	Energy
g_D, g_A	The degeneracy factor for the impurity level
h	Planck's constant
I_o	Dark saturation current
I_h	Hole current
I_e	Electron current
I_L	Light generated current
I_S	Reverse saturation current
J	Current density
J_o	Saturation current density
J_L	Junction photo current density
J_{sc}	Short circuit current density
J_m	Maximum current density
k	Boltzmann's constant
L_n, L_p	Diffusion length for electron and hole
M_C, M_V	Number of equivalent minima in the conduction, valence band
m_e, m_h	Effective mass of electron, hole
μ_e, μ_h	Mobility of electron, hole
n	Electron density
n_o	Refractive index of air
n_i^2	Intrinsic carriers concentration square
xn, xp	Thickness of (n, p)type layer of junction
N_A, N_D	Acceptor and donor doping density
N_C, N_V	Density of states in the conduction and valence band
p	Hole density
P	Momentum
P_{in}	Input power (Incident irradiance per unit area)
P_{out}	Output power
q	Electron charge
R	Recombination rate
R_S	Series resistance
R_{SH}	Shunt resistance
R_{min}	The minimum reflectivity
S_n, S_p	Surface recombination of n-type and p type
T	Temperature
t_j	Thickness of junction
V_m	Maximum voltage
V_t	Thermal voltage
V_{oc}	Open circuit voltage
W	Depletion region
χ	Electron affinity

χ_0	Electron affinity at 0 K
x_L	Absorption length
α	Absorption
α, β	Material parameters
ε	Dielectric constant
ρ	Resistivity
τ_n, τ_p	Lifetime of minority electrons, holes
η	Efficiency

SIMULASI, FABRIKASI DAN PENCIRIAN SALUTAN PELBAGAI LAPIS SEL SOLAR

ABSTRAK

Kajian ini merupakan kombinasi antara simulasi teori dan eksperimen fabrikasi salutan pelbagai lapis sel solar. Pada bahagian teori, simulator ISE-TCAD (versi 9.5) digunakan. Manakala model simulasi dicipta/dibina dengan menggunakan teori-teori relevan mengenai sel solar dan data eksperimen kemudiannya diaplikasi untuk mengesahkan keputusan daripada simulasi.

Proses fabrikasi solar sel dijalankan dimana ia melibatkan salutan lapisan penteksturan dan lapisan anti-pantulan. Untuk proses penteksturan, larutan alkali (KOH) dan asid ($\text{HNO}_3 + \text{HF} + \text{CH}_3\text{COOH}$, 15:3:2) telah digunakan. Manakala untuk lapisan anti-pantulan ZnO/TiO_2 dan silicon berliang telah digunakan untuk meningkatkan penangkapan cahaya daripada struktur sel solar. Seterusnya, penteksturan melalui larutan asid dan lapisan anti-pantulan berganda (ZnO/TiO_2) dibuat pada bahagian atas dan lapisan pantulan pada bahagian bawah untuk mereka bentuk suatu corak salutan pelbagai lapis sel solar yang baru Mofologi permukaan dan ciri-ciri struktur sampel-sampel dikaji dengan menggunakan mikroskop pengimbas electron (SEM) dan mikroskop daya atom (AFM). Seterusnya, pengukuran spektroskopi Raman dan Fotoluminesen dijalankan pada suhu bilik. Manakala pantulan optik pula diperoleh daripada ujikaji menggunakan Filmetrics (F20). Ketumpatan arus-voltan (J-V) pada salutan pelbagai lapis sel solar diukur di bawah keadaan sampel diterangi dengan kuasa $80 \text{ mW}/\text{cm}^2$.

Keputusan simulasi menunjukkan peningkatan nilai sel solar iaitu mempertimbangkan peningkatan oleh litar voltan terbuka yang mengeluarkan

kecekapan yang tinggi (15.94%) bagi silikon berongga dan 8.84% untuk silicon pukal.

Keputusan daripada eksperimen tekstur larutan asid dan salutan ZnO/TiO₂ menunjukkan kecekapan yang lebih (12.04%) berbanding eksperimen tekstur menggunakan alkali dan salutan ZnO/TiO₂ (10.31%). Seterusnya keputusan eksperimen juga menunjukkan bahawa silikon n-type (100) berongga boleh meningkatkan pertukaran kecekapan sebanyak 15.42% berbanding silikon berongga p-type (100), dimana kecekapannya hanya 11.23%. Akhirnya ketumpatan-voltan bagi struktur termasuklah tekstur berasid bagi silikon n-type (100) dan salutan anti-pantulan ZnO/TiO₂ pada bahagian atas dan salutan pantulan pada bahagian bawah menunjukkan bahawa nilai bacaan litar ketumpatan arus singkat adalah 29.97 mA/cm², manakala nilai bacaan litar voltan terbuka adalah 0.55V dan kecekapan penukaran sel solar adalah 15.84%.

Keputusan yang diperolehi telah jelas menunjukkan kepentingan kajian dengan menggunakan simulasi dan eksperimen untuk mengkaji struktur baru sel solar.

SIMULATION, FABRICATION AND CHARACTERIZATION OF MULTILAYER COATED SOLAR CELLS

ABSTRACT

This work is a combination of a theoretical simulation and an experimental fabrication of multilayer coated solar cells. ISE-TCAD simulator, release 9.5 was used in the theoretical part. A simulation model was established by employing known theories relevant to solar cells and the experimental data was applied to validate the simulation results.

The solar cells were fabricated by means of texturing and antireflection coating. For texturing, alkaline (KOH) and mixture acidic solution ($\text{HNO}_3+\text{HF}+\text{CH}_3\text{COOH}$, 15:3:2) were used. For antireflection coating, ZnO/TiO_2 and porous silicon were used to increase the light trapping of solar cell structures. Furthermore, texturing through an acidic solution and double antireflection coating (ZnO/TiO_2) at the top and a reflection coating at the bottom were used to fabricate a new structure of multilayer coated solar cell.

Surface morphology and structured properties of samples under this study were characterized using Scanning Electron Microscopy (SEM) and Atomic Force Microscopy (AFM). Raman and Photoluminescence (PL) measurements were carried out at room temperature. Optical reflectance was experimentally obtained using Filmetrics (F20). Current density-Voltage (J-V) of multilayer coated solar cell was measured under illumination conditions of $80 \text{ mW}/\text{cm}^2$.

The simulation results showed an increase in the values of the solar cells which is ascribed to the increase in the open circuit voltage that produced high efficiencies of (15.94 %) for porous silicon (PS) and (8.84 %) for the silicon as grown (c-Si).

The experimental results of acidic solutions texturing and ZnO/TiO₂ coating revealed higher efficiency (12.04%) compared with alkaline texturing and ZnO/TiO₂ coating (10.31%). The experimental results also showed that porous silicon n-type (100) increased the conversion efficiency 15.42% compared with porous silicon p-type (100) whose efficiency was 11.23%. Finally, the current density-voltage of the structure which includes acidic texturing of silicon n-type (100) and antireflection coating ZnO/TiO₂ at the top and the reflection coating at the back showed that the short circuit current density was 28.9 mA/cm², open circuit voltage was 0.55 V and the conversion efficiency of solar cell was 15.76 %.

Overall, these results obtained clearly indicate the advantage of using simulation and experimental study to investigate new structures of solar cells.

CHAPTER 1

INTRODUCTION

1.0 Overview

The first silicon solar cell has been made by Russell Ohl in 1941. In 1954, three other American researchers, G.L. Pearson, Daryl Chapin, and Calvin Fuller, demonstrated a further-refined silicon solar cell capable of achieving energy conversion efficiency in direct sunlight of 6% (Chapin, et al., 1954). By the late 1980s, silicon cells as well as those made of gallium arsenide, with efficiencies of more than 20% had been fabricated. In 1989 a concentrator solar cell, a type of device in which sunlight is concentrated onto the cell surface by means of lenses, achieved an efficiency of 40% (Swanson, 2000). The U.S. department of energy, along with an industry consortium, began operating a solar power tower project in 1999; this project demonstrated how solar energy can be stored efficiently and economically so that power can be produced even when the sun is not shining.

In 2000, the first solar plant was established to produce solar panels to generate 100 megawatts of power each year. After that in 2001, the National Space Development Agency of Japan (NASDA) announced plans to develop a satellite-based solar power system that would beam energy back to Earth. A satellite carrying large solar panels would use a laser to transmit the power to an airship at an altitude of about 12 miles which would then transmit the power back to Earth. In 2002, NASA successfully conducted tests on a solar-powered, remote-controlled aircraft called Pathfinder Plus. In these tests, the researchers used the aircraft as a high-altitude platform for telecommunications technologies. In 2007, a novel technology has been introduced by the University of Delaware to achieve a solar cell of

efficiency of 42.8 percent from sunlight at standard terrestrial conditions, Science daily (Anonymous, 2007).

1.1 Materials consideration

The number of materials considered for the fabrication of solar cells and modules is already large and is still growing. The original choices were mainly motivated by material availability and processing possibilities, but the increased attention recently in solar cells has triggered a more systematic search for new materials and cell structures that may fulfill the ultimate requirements of efficiency, cost, stability and environmental effects (Burgelman, et al., 2004). The physical properties of materials which affect the solar cell performance include the bandgap, absorption and multilayer. Therefore, these properties will be discussed in following subsections.

1.1.1 Bandgap energy

The bandgap energy (E_g) of materials is always one of two types, either direct bandgap or indirect bandgap as shown in Figure 1.1. In direct bandgap energy, the electrons in the conduction band minima and the holes in the valence band maxima have the same momentum. The probability of a band to band radiative transition for the direct bandgap semiconductor is high since the momentum is conserved upon recombination. In contrast, in indirect bandgap energy, the electrons in the conduction band minima have different momentum from the holes in the valence band maxima; therefore, the momentum is not conserved. In an indirect semiconductor, an electron should change its momentum before recombining with a hole. A phonon is required to participate in the recombination event so that the

electron can change its momentum to make a transition in the indirect bandgap semiconductor (Goetzberger, et al., 1998). This results in a significantly lower recombination probability for a band to band transition to occur in the indirect bandgap semiconductor. This fact is particularly evident when comparing the direct bandgap in nitride group to indirect bandgap of silicon.

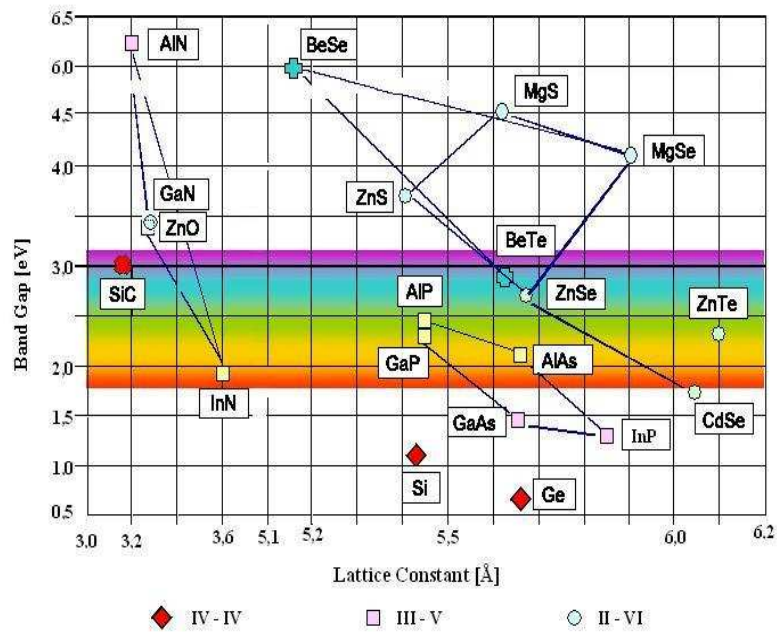


Figure 1.1: Bandgap of some common semiconductor materials [Adapted from Wu, et al., 2003].

At temperatures above absolute zero, the electrons may possess enough thermal energy (at least E_g) to be excited across the forbidden energy gap into the conduction band. This occurrence is less likely to happen if the bandgap energy is large as in insulators. In conductors, the conduction band and the valence band overlap and conduction of the electrons occurs, even at absolute zero. This situation explains why insulators are considered as poor conductors of the electrical current whereas, conductors are not.

1.1.2 Absorption

Each semiconductor is characterized by bandgap energy (E_g). The energy needs to free an electron from the nucleus to create one electron-hole pair. This energy can be supplied in the form of light. Each light photon has energy $h\nu$, where h is the Planck's constant and ν is the frequency of the light wave (Hu & White, 1983). The energy $h\nu$ can be expressed as

$$h\nu(eV) = h \frac{c}{\lambda} = \frac{1.24}{\lambda(\mu m)} \quad (1-1)$$

where c is the speed of light and λ is the light wavelength. For example, each light photon of $0.62 \mu m$ wavelengths has energy equal to 2 eV. Semiconductor can absorb photons having $h\nu > E_g$. The energy of each absorbed photon is consumed by raising a valence band electron into the conduction band and creating one electron and one hole.

Each photon having $h\nu$ greater than E_g is capable of generating one and only one electron-hole pair. The excess energy is dissipated as heat. Photons with $h\nu < E_g$ are basically not absorbed by the semiconductor and cannot generate electron-hole pairs (Mckelvey, 1966). This fact plus the spectral distribution of solar radiation lead to the conclusion that the maximum photon-absorption rate or carrier-generation rate per unit area is a function of bandgap energy of the semiconductor (Hu & White, 1983). To elaborate more about the absorption in semiconductors, the absorption in direct and indirect bandgap energy will be discussed in the next subsection.

1.1.2.1 Absorption in a direct bandgap

The absorption process is best demonstrated in direct bandgap semiconductors. As seen from Figure 1.2, the minimum energy of the conduction band in relation to the crystal momentum p lies directly above the maximum of the valence band.

The probability of this absorption process naturally depends upon the density of electrons and holes. The absorption is zero when the electron is at the edge of the band, and it increases significantly when the electron moves away. It is clear that at higher photon energy, the absorption probability increases significantly because the photon energy is sufficient for the absorption even when the crystal momentum lies outside the min/max situation.

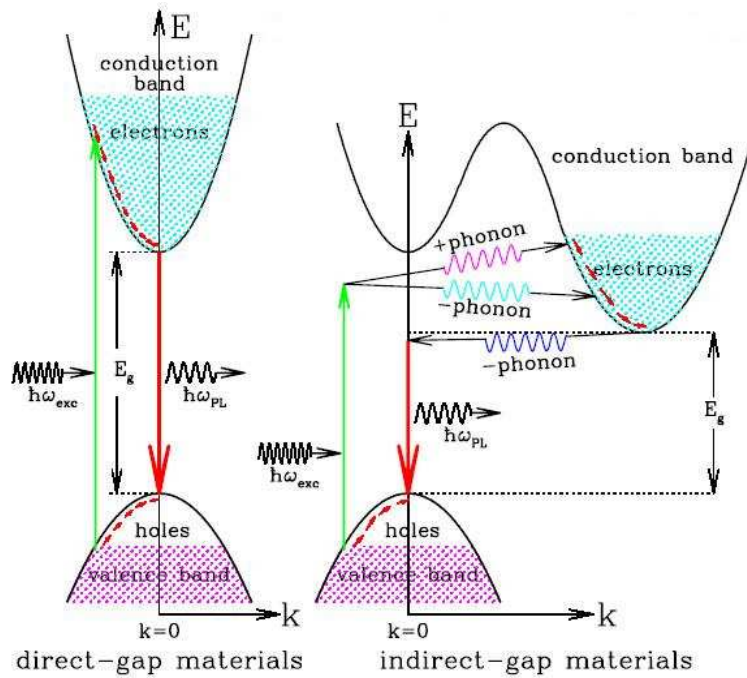


Figure 1.2: Energy versus crystal momentum in a direct and indirect bandgap [Adapted from Nakamura & Chichibu, 2000].

The following expression gives the absorption coefficient in direct bandgap energy:

$$\alpha_{\lambda} = C \left[h \frac{c}{\lambda} - E_g \right]^{1/2} = C (h\nu - E_g)^{1/2} \quad (1-2)$$

where constant C is approximately 2×10^4 for direct semiconductor if the absorption coefficient α is given in cm^{-1} (Pankove, 1971).

A semiconductor with a direct bandgap shows that an electron can shift from the lowest-energy state in the conduction band to the highest-energy state in the valence band without a change in crystal momentum.

1.1.2.2 Absorption in an indirect bandgap

The situation in an indirect semiconductor is different. In this case the minimum of the conduction band and the maximum of the valence band lie at different crystal momentum. The direct transition from the valence band to the conduction band requires a higher energy level than $h\nu = E_g$. It is, however, possible to excite towards the conduction band minimum if the necessary change in momentum can be induced by thermal vibrations in the lattice, i.e. a phonon. A phonon itself has low energy in comparison with a photon that has very high momentum (Green & Keevers, 1995). The important point here is the fact that the possibility of absorption is much lower than that of a direct semiconductor due to the involvement of two different particles. Silicon is the most common solar-cell material, despite the fact that it is an indirect bandgap and therefore does not absorb light very well. To solve the limitation of silicon absorption, the silicon solar cell is normally made much thinner, but for thinner silicon cells, much of the light (particularly in the infrared) can simply pass through. The using of high reflectivity coating at the back surface of silicon could prevent the light escaping from the rear surface and double the light path. The rear surface is typically metalized with aluminum or silver and can provide reflectivity of over 95% (Nelson, 2003).

The absorption spectrum of an indirect bandgap material usually heavily depends on temperature than that of a direct material because at low temperatures there are fewer phonons. Therefore, it is less likely that a photon and phonon can

simultaneously be absorbed to create an indirect transition. For example, silicon starts to transmit red light at liquid helium temperatures because red photons do not have sufficient energy for a direct process (Rosencher & Vinter, 2002).

1.1.3 Multilayer

The amount of work done per photon could clearly be increased if photons of different energies could be absorbed preferentially in cells of different bandgap. If the solar spectrum could be split up and channeled into converters of different bandgap this leads to absorb most of the incident light in multi-bandgap design. A more practical strategy is to stack different bandgap in optical series and allow the wider bandgap materials at the top to filter out most of the high energy photons; while, less energetic photons pass through smaller bandgap materials at the bottom as illustrated in Figure 1.3 (Dharmadasa, 2005).

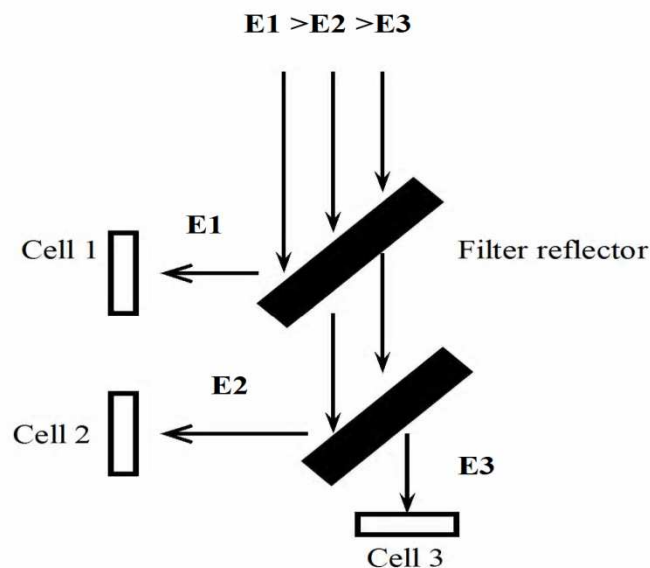


Figure 1.3: Spectrum- splitting schemes to achieve high conversion efficiencies.

The main aim of a multilayer solar cell is to absorb a lot of amount of the solar spectrum and hence increasing the efficiency of the device by increasing the electric current. The approach is to fabricate p-n, p-i-n, p-n / p-n or any other diode structure with different bandgap semiconductors and connect them to enhance the PV conversion. The multiple bandgap in solar cells can convert a larger range of the solar spectrum to electric power as compared to single bandgap solar cells which has significantly higher limiting efficiencies as modeled by Henry (1980). The larger spectral range of these devices also requires a more broadband antireflection (AR) coating.

The most popular material silicon has a less favorable bandgap (1.12 eV). Recent developments in semiconductor materials indicate that the indium gallium nitride $\text{In}_x\text{Ga}_{1-x}\text{N}$ alloy which has the bandgap can be varied continuously from 0.77 to 3.4 eV is a promising material for solar cell energy conversion (Wu, et al., 2002).

1.2 Rules of device structure

When incident photons strike a semiconductor, they may excite an electron out of its energy level and consequently leave a hole. This process is known as electron-hole pair generation. Electron-hole pairs are also constantly generated from thermal energy in the absence of any external energy source. Electron-hole pairs are also apt to recombine (Landsberg, et al., 1987). Conservation of energy law requires that the electron-hole pair is to be recombined where the difference between the electron energy and the bandgap energy will be lost in the form of emission of thermal energy (in the form of phonons) or radiation (in the form of photons) as shown in Figure 1.4.

The device which consist of a semiconductor p-n junction diode, is made of a p-type semiconductor, containing mobile positive charges called holes (which correspond to the vacant electron sites), and an n-type semiconductor, containing mobile electrons (the electron has a negative charge). The densities of holes and electrons in the respective regions are made extremely high by doping a large amount of the appropriate impurities with an abrupt transition from one region to the other. In semiconductors, the conduction band of mobile electrons is separated from the valence band of mobile holes by an energy gap which corresponds to a forbidden region.

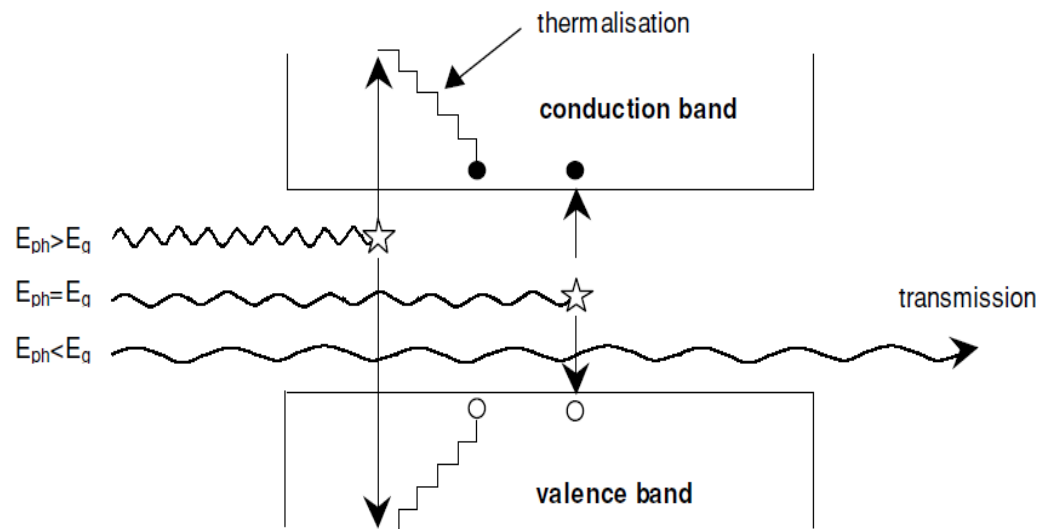


Figure 1.4: The generation and recombination phenomenon in semiconductors.

The electromagnetic radiation of solar energy can directly be converted to electricity through photovoltaic effect. Being exposed to the sunlight, photons with energy greater than the bandgap energy of the semiconductor are absorbed and they create some electron-hole pairs proportional to the incident irradiation (Licht, 2001). Under the influence of the internal electric fields of the p-n junction, these carriers

are swept apart and they create a photocurrent which is directly proportional to solar insolation.

1.2.1 Single-junction solar cell

Photovoltaic energy conversion in solar cells consists of two essential steps. First, absorption of light generates an electron-hole pair. The electron and hole are then separated by the p-n junction of the device and very quickly sweeps electrons to the negative terminal and holes to the positive terminal thus generating electrical power.

When the sun light falls down on the semiconductor p-n junction, the new hole-electron pairs in the p-n junction can be generated. However, the charges are built up on both sides of the junction and consequently an electric field is created. This result in creating a diode that promotes the charge flow (known as drift current) the charge carriers generated in this region to contribute to the circuit current of the solar cell.

At one-sun concentrations, the single-junction solar cell provides limited efficiencies about 25 % or less than this value (Dicker, et al., 2002).

1.2.1.1 Homojunction

A homojunction is a semiconductor interface that occurs between layers of similar semiconductor materials (equal bandgaps). A homojunction occurs at the interface between an n-type and p-type semiconductor such as silicon. The electrostatic barrier region of homojunction cells is the (charge separation engine). It is either a p-n type or a p-i-n type. These barriers break symmetry and make one direction different from the other thereby causing charge separation and current flow (Sze and Ng, 2007).

1.2.1.2 Heterojunction

Heterojunction (HJ), is two different materials with different bandgaps form a junction, proved to be more efficient (Kabir et al., 2010).

One of these materials of an HJ must obviously be an absorber. The other one may be an absorber too, or it may be a window material; i.e., a wider-gap semiconductor that contributes little or nothing to light absorption, but it is used to create the heterojunction and to support the carriers transport. Window materials collect holes or electrons, function as majority-carrier transport layers and can separate the absorber material from deleterious recombination at the contacts. The physical structure of heterojunctions fits into one of two types: planar or bulk. It is made up of two semiconductor materials that form the active layer (an absorber-absorber or an absorber-window combination) (Bube, 1980).

1.2.2 Multi-junction solar cell (Tandem solar cells)

The collection of light-generated carriers does not by itself give rise to power generation. In order to generate power, a voltage must be generated as well as a current. The collection of light-generated carriers by the p-n junction causes a movement to the electrons toward the n-type side and holes toward the p-type side of the junction.

A multi-junction solar cell (or tandem solar cell) is a *photovoltaic cell* that works in a fashion similar to those for *single-junction cells*. The multiple electric fields are created in every junction to drift the electrons towards n-region and the holes towards p- region in every junction. This leads the charge carriers to generate the current of the solar cell. In this configuration, each junction, that is defined in a different semiconductor layer, possesses a different bandgap and tuned to a different

wavelength segment of the solar spectrum (Isomura, et al., 2002). Thus high energy photons are absorbed in the top junction, generating electron-hole pairs, and less energetic photons pass through to the lower junctions where they are absorbed and they generate additional electron hole pairs. The current generated in the junctions is then collected at ohmic contacts formed at the top and bottom of the solar cell. By employing compound semiconductor materials in this arrangement, the solar cell makes more efficient use of the available energy in the solar spectrum and yields substantially higher conversion efficiency than single junction solar cells formed by silicon.

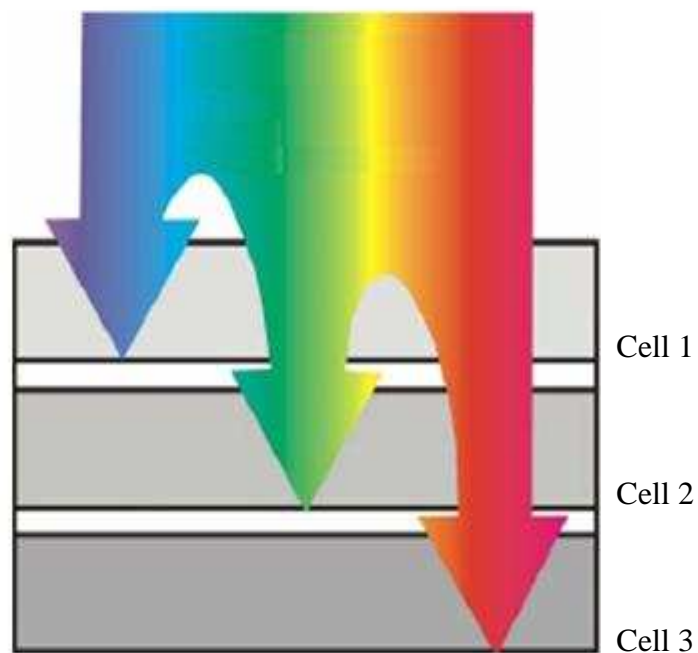


Figure 1.5: Multi-junction solar cell design [Adapted from solar server (Anonymous, 2009)].

In Figure 1.5, the top layers are designed to absorb high-energy photons while the low-energy photons are transmitted to be absorbed by the lower layers of the cell. The multi-junction design is capable of increasing the solar cell efficiency up to 40 percent (Yamaguchi, et al., 1987).

1.3 Simulation as a tool

Many programs had been used in solar cells designs. In this study, the researcher used a simulation program called ISE-TCAD simulator to make multilayer coated solar cells. The use of computer simulation has become necessary in the design and analysis of solar cells due to the complicated physical mechanisms that govern photovoltaic device (PV) (Burgelman, et al., 2004). Optimizing the efficiency of a solar cell is a significant challenge as it is often costly and requires more efforts in manufacturing. Therefore, such simulation programs have become a powerful tool in quantifying and minimizing the losses in solar cell performance; they also provide faster creation of solar cell manufacturing. The quantification of limiting losses in solar cells was made possible by the advanced physical models and the improved material parameter database of this program (Dicker, et al., 2002). The numerical modeling tools have increasingly become useful due to the development of processing and computing resources that are available today.

Simulation modeling of solar cell design will be able:

1. To achieve a good insight or understanding of the device performance and to capture theoretical knowledge of photovoltaic cell
2. To design a structure to provide information that is difficult or impossible to measure in solar cell fabrication
3. To optimize the solar cell in a much quicker and cheaper way than the experimental work

1.4 Research motivations

A lot of work has been done in simulating and fabricating solar cells, but there is still a dire need for much more developing skills and techniques to make low cost, simple and super-efficient ones. Materials presently used for photovoltaics include silicon, cadmium telluride, and gallium arsenide (Jacobson, 2009). The most commonly used semiconductor material for the construction of photovoltaic cells is silicon, but there are certain physical processes that restrict the silicon solar cell efficiency.

In general the high efficiency solar cell fabrication requires hard work and high cost and is time consuming. Because the pure silicon is shiny, it can reflect up to 35 percent of the sunlight. The incident light energy, which is higher or lower than the bandgap energy of a semiconductor material, can be transferred to waste energy. Because of the abrupt discontinuity of the lattice structure on the silicon surface, a large number of localized energy states or generation-recombination center may be introduced at the surface region.

For detailed understanding and further optimization, computer modeling has become an essential tool which can improve the solar cell structure by saving time, cost and effort. The simulation of the electrical and optical behavior of semiconductor devices is considered as an essential tool for both the improvement of existing devices and the development of new ones. Numerical modeling is increasingly used to provide insightful details about the physical operation of solar cell structures.

In a solar cell design, light absorption, surface recombination and reflectivity play very critical roles in enhancing the physical characteristics. Many methods have been proposed to further enhance the performance, including a reduction of

reflectance from the solar cell surface. Minimizing reflectivity losses through the top surface of a solar cell are achieved by combining surface texturing and an antireflection coating (ARC). Antireflection coating layers can be added on the silicon surface to remove the dangling bond on the silicon surface and also can be used to serve as guttering centers to reduce the impurity levels of the silicon substrate (Menna & Tsuo, 1997). In multilayer coated the multiple bandgap systems are capable of better matching and utilizing the incident solar radiation. Furthermore, the multiple bandgap design can provide more efficient matching of the solar spectra (Henry, 1980). The primary requirement for the materials to be used for solar cell is a bandgap matching with the solar spectrum. The porous silicon can be used to improve the photovoltaic cell structure because it exhibits electroluminescent and photoluminescent properties similar to those properties of a semiconductor with a direct bandgap energy (Canham, 1990).

1.5 Objectives of the study

This work is a theoretical simulation and experimental fabrication of multilayer coated solar cells. The design and performance evaluation of a multilayer coating was made by using ISE-TCAD simulator. The simulation and fabrication goals are listed in the subsections below.

1.5.1 Simulation goals:

1. To develop the physical simulation programs to quantify and minimize efficiency losses in the solar cells
2. To simulate the effect of the antireflection coating for porous silicon solar cells

1.5.2 Experimental goals:

1. To apply a more effective texturing as an alternative to the alkaline texturing (KOH) by using mixture acidic solution ($\text{HNO}_3 + \text{HF} + \text{CH}_3\text{COOH}$, 15:3:2)
2. To determine the effectiveness of a single-layer and double-layer as antireflection coatings (ARC) for enhancing the optical properties of the solar cell surfaces
3. To determine the effectiveness of the type and orientation of the porous silicon as antireflection coating in solar cells
4. To determine the effectiveness of using the acidic solution texturing with double layer ZnO/TiO_2 as antireflection coating on top a silicon surface and the porous silicon as reflector coating in rear silicon surface in a solar cell

1.6 Originality

The ISE-TCAD simulation program has been used to develop the silicon solar cell with a multilayer coating. This is the first study used a double layer coating of ZnO/TiO_2 instead of single layer SiO_2 to enhance the solar cell absorption. New solar cell structure consisting of ($\text{HNO}_3 + \text{HF} + \text{CH}_3\text{COOH}$, 15:3:2) solution texturing, a double layer $\text{ZnO}_2/\text{TiO}_2$ top antireflection coating and PS as back reflector coating was introduced effectively.

1.7 Outline of the thesis

Briefly, the content of this thesis are presented as follows:

Chapter 1 describes the history of solar cell, materials consideration, rules of device structure, simulation as a tool and fabrication.

Chapter 2 deals with a brief literature review of the research regarding the simulation, texturing, antireflection coating and multi-junction (tandem) solar cells.

Chapter 3 presents the relevant theories and the basics of physics for a photovoltaic cell.

Chapter 4 covers advanced physical models and improved material parameter database by using ISE-TCAD software.

Chapter 5 covers the equipment, instrumentation and techniques, which were used in processing and characterizing.

Chapter 6 includes the experimental methodologies.

Chapter 7 presents the experimental observations, calculations and explanations of the findings together with the theoretical results.

Chapter 8 explains the conclusions and future studies.

CHAPTER 2

LITERATURE REVIEW

2.0 Introduction

An optimum solar cell structure typically has *light trapping* where the optical path length is several times the actual device thickness. The optical path length of a device here refers to the distance where an unabsorbed photon may travel within the device before it escapes out of the device. This is usually defined in terms of device thickness. For example, a solar cell with no light trapping features may have an optical path length of one device thickness; while a solar cell with good light trapping may have an optical path length of 50 times, which means that light bounces back and forth within the cell many times (Yablonovitch & Cody, 1982).

The fabrication of silicon solar cells has overcome a major problem associated with the light trapping effect by designing multilayer solar cells (Staebler & Wronski, 1977). The most common way to incorporate light-trapping is the use of textured and antireflection coating cells. Such a use of texturing and antireflection coating in the solar cells is very difficult or even impossible to handle by simple optical analysis. More advanced numerical analysis tools are required to deal with the optical designs and analyses of these cells and modules (Sopori, et al., 1998).

Therefore, this chapter will review the literature related to the simulation programs and the multilayer coating technique which include the texturing and antireflection coating solar cells.

2.1 Simulation programs

In order to develop the technology of solar cells further, numerical modeling and simulation of devices can be used. Simulation programs have been used previously as a valuable tool to enhance the understanding of device operation and they are important because through such simulation programs the solar cells can be fabricated at low cost (Tuttle, et al., 1995; Burgelman et al., 2004). Several software packages of this kind of simulations have been developed (Burgelman, et al., 2000; Froitzheim, et al., 2003).

Fan, et al. (1982) encouraged using tandem solar cells based on computer analysis. As soon as simulation software became available in the mid-1980s, solar cell engineers realized its potential for optimizing their designs and followed by their fabrications. The reflection losses have been modeled using a silicon wafer with a thin silicon oxide and silicon nitride antireflection coating at standard solar spectrum (AM1.5). The results showed that antireflection coating is sufficient to trap the most of incident light. It has been proved that the two layer oxide/nitride stacks are an effective ARC for single junction silicon solar cell (Buiea, et al., 2004).

A new model of a multilayer solar cell has been proposed; the cell consist of four layers of opposite conductivity, including a frontal layer of n-type 6H-SiC to absorb high energy photons and a back layer of p-type $\text{Si}_{0.8}\text{Ge}_{0.2}$ to absorb low energy photons of the solar spectrum. The other two layers are p-type silicon layer and n-type silicon layer (Bouzidi, et al., 2006).

The interest in thin-film solar cells has sharply increased due to its promising characteristics for large scale production and thus cost reductions. Ulf and Marika (2009) have shown how thin-film hetero-junction solar cells can be modeled and simulated in two dimensions, using a finite element method.

The trap-assisted tunneling theory was developed to describe the tunneling of charge carriers via bandgap energy levels in structures based on hydrogenated amorphous silicon and microcrystalline silicon. Models that were verified on n/p single junctions were applied in the tunnel recombination junction area of a tandem solar cell. Thus, it is possible to study a multi-layer solar cell without separately simulating any of its components (Vukadinovic, et al., 2001).

Simulation has yielded good results to the limiting characteristics of a GaP solar cell. Shunt resistance, series resistance, doping profile, and material life time have yielded good agreement with laboratory results. Top surface recombination and p-type material quality are believed to be the limiting factors in improving the cell efficiency (Allen, et al., 2010). To improve the top surface characteristics, heterojunction cap (GaAlAs) has been used based on GaAs material (Woodall & Hovel, 1972).

2.2 Multilayer coating techniques

The concept of light trapping via multilayer process has been introduced for a long time (Prince, 1955); it has been suggested that light absorption can be improved by using many methods of multilayer by developing structures using, for example, texturing or antireflection coatings (ARC) and these two methods can also be applied altogether to enhance the absorption of incident light. The following sub-sections will discuss these two methods.

2.2.1 Texturing

Hu and Kerr (1967) have shown that it is possible to make structures on silicon using wet chemical etching. The use of alkaline texturing to make light trapping

structures has been proven to be effective, and it has become an essential step in manufacturing solar cells based on silicon. However, due to the anisotropic nature of the alkaline textures, their application is limited to monocrystalline wafers of (100) orientation. This anisotropic nature is believed to be due to the different etching rates of crystalline orientation (Seidal, et al., 1990), but the exact interpretation is still a matter of debate (Stefancich, et al., 2001). To overcome this limitation, different methods have been introduced as alternative texturing techniques (Zechner, et al., 1997), such as mechanical texturing which employs a mechanical means to define textures on the wafer. Although high efficiency solar cells have been processed using this technique (Weber, 2004), this method is limited as an industrial candidate due to the fragile nature of silicon wafers (Gerhards, et al., 2000).

Plasma and Reactive Ion Etching (RIE) have also been used where an ion beam is used to etch structures using predefined mask patterns. Here, the wafer surface is etched using an ion beam (Rubya & Zaidi, 2002). These two methods are known to cause severe damage to the etched surfaces and this problem can be treated chemically (Kumaravelu, et al., 2004).

Texturing through the use of acidic solution has also been applied (Zhao, et al., 1999). Due to its isotropic nature, this method can be used irrespective of the crystalline orientation of the base material, a feature that makes it most favorable in the texturing of multicrystalline silicon cells (Macdonald, et al., 2004). Moreover, the alkaline, RIE, and plasma texturing are very beneficial in passivating stress effects or surface damage (Zaidi, 2000). Being isotropic, acidic texturing has been used to produce geometrical textures as well. Recent results showed that this technique is as effective as the mostly used alkaline texturing (Schultz, et al., 2003).

2.2.2 Antireflection coating

Antireflection coating is another key factor in solar cell processing, where a thin film of quarter wavelength type or material of intermediate refractive index between the cell base material and the uppermost layer air/glass is used (Cid, 1998). Several transparent and high refractive index material films have already been applied to ARC techniques, e.g. SiO (n = 1.8–1.9), SiO₂ (n = 1.44), Si₃N₄ (n = 1.9), TiO₂ (n = 2.3), Al₂O₃ (n = 1.86), Ta₂O₅ (n = 2.26), SiO₂–TiO₂ (n = 1.8–1.96) and ZnS (Kishore, et al., 1992). Kern and Tracy (1980) have observed an increase of 44% in the cell efficiency after spraying TiO₂ single-layer ARC.

Green (1984) has used MgF₂/ZnS double-layer (ARCs) on Si cells with 19.1% efficiency. Coatings are either deposited such as TiO₂, ZnS or grown by thermal such as SiO₂ or by electrochemical etching such as porous silicon. Single and double layer antireflection coating has been applied using different materials, such as SiO₂ and TiO₂ (Zhao, et al., 1994). The mixture of SiO₂ and TiO₂ is particularly interesting because it involves two oxides with quite different refraction indices (i.e., around 1.45 and 2.45 for bulk SiO₂ and TiO₂ oxides respectively) (Chen, et al., 1996) and bandgap energies (8.5 and 3.2 for SiO₂ and TiO₂ respectively) (Sze, 2001 ; Gracia, et al., 2004). SiO₂/TiO₂ thin films have been prepared by using different methods including sol–gel or different kinds of chemical vapor deposition procedures (Song, et al., 2002; Kamada, et al., 1991). Double layer coating have been used in space because the solar cells used are of high efficiency; while single layer coatings have been used for commercial purpose because such solar cells are of low costs (Richards, 2003).

Porous silicon (PS) was also used as an ARC layer and found to be effective as it acts as a passivation layer as well (Ludemann, et al., 2000). It was discovered in

1990 that PS formed on crystalline-silicon wafers using electrochemical etching exhibits electroluminescent and photoluminescent properties similar to those properties of a semiconductor with a direct energy gap (Canham, 1990). PS layers can be easily produced on single or multi-crystalline silicon surfaces by electrochemical or stain etching at a very low cost. Several possible methods of using PS to improve the performance of crystalline silicon solar cells have been proposed. It was shown that PS etched has excellent antireflection properties (Tsuo, et al., 1994). PS may also serve as a wide bandgap absorber in a multiple junction cell structure, with crystalline silicon as a substrate or as guttering centers to reduce the impurity levels in a silicon substrate (Menna & Tsuo, 1997). In thin film silicon solar cells, PS has been demonstrated as a back-surface reflector (Zettner, et al., 1998).

Attempts were even made to use two PS layers with two different bandgaps in a three bandgap solar cell on a silicon wafer (Kore & Bosman, 1999). Although PS has not been used yet in any commercial silicon solar cell, it remains a potential resource for improving the crystalline silicon photovoltaic technologies. The large specific surface area of PS and chemical properties of the surface has an effect on the electrical, optical and mechanical properties.

CHAPTER 3

THEORETICAL FRAMEWORK OF SOLAR CELL

3.0 Introduction

The physical concepts of the operative photovoltaic cells such as, electromagnetic spectrum, the band theory of solid state, resistance, electric field, type of semiconductors, p-n junction in semiconductors and solar cell principles will be discussed in this chapter through the subsequent sections.

3.1 Electromagnetic spectrum

The whole energy carried by photons is referred to as electromagnetic (EM) energy which is possible to be transferred to wavelength and frequency. Ranges of this spectrum are from the shortest wavelength to the longest and are referred to as gamma rays, x-rays, ultraviolet, visible light, infrared, microwaves, and radio waves.

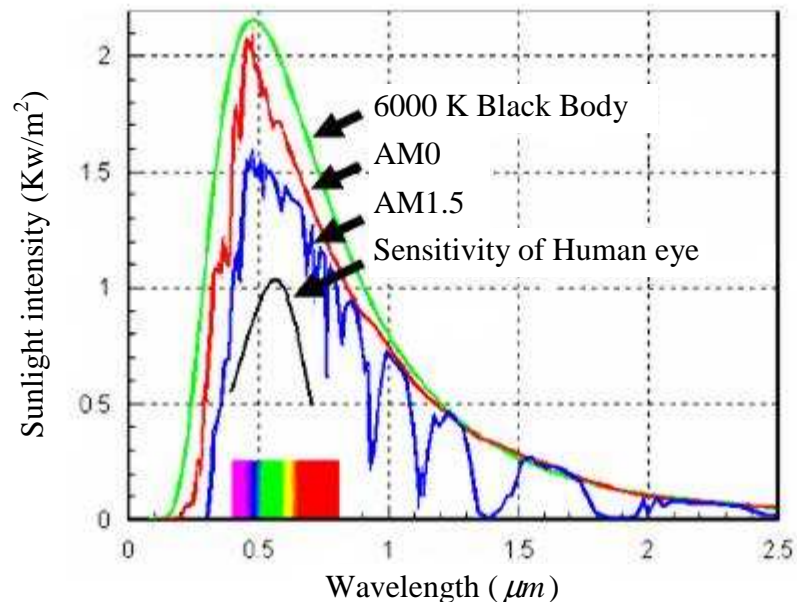


Figure 3.1: Electromagnetic spectrum of cosmic rays [Adapted from Moller, 1993].

The solar energy, that reaches the surface of the earth, is determined by the ratio of the diameters of the sun and the earth and their distance apart. If we disregard the deviation that arising from the rotation of the earth around the sun, the most recent measurement of the radiation power outside the atmosphere is $D_0 = 1.353 \text{ kW/m}^2$. The value D_0 is known as the solar constant (Thekeara, 1970).

Air Mass (AM) gives information about the air mass amount of the incident radiation. The terms AM0 and AM1.5 used in Figure 3.2 are specific radiation conditions which mean:

AM0 : the extraterrestrial radiation, e.g. applicable to satellites in space

AM1 : the vertical incidence of sunlight at the equator at sea level

AM1.5: sunlight radiating through an air mass 1.5 times greater than the vertical case.

The energy carried by a photon is calculated by multiplying the frequency of the photon by a universal constant (h) called Planck's constant as shown below:

$$E = h\nu \quad (3-1)$$

where E is the energy in joules or electron volts, h is Planck's constant ($6.6262 \times 10^{-34} \text{ J-s}$, or $4.1357 \times 10^{-15} \text{ eV-s}$) and ν is the frequency of the photon in Hz .

3.2 The band theory of a solid state

To understand the electrical properties of a material, it is helpful to consider the two bands commonly referred to as the valence band and conduction band. The valence band encompasses the energy levels at which most of the electrons at absolute zero will be found. The electrons found in the higher-energy conduction band are considered free electrons. These free electrons of the atom share with the other atoms of the material. Therefore, they have a very high mobility action. As a